Rapidly Reversible Organic Crystalline Switch for Conversion of Heat into Mechanical Energy

Madushani Dharmarwardana,[a,†] Srimanta Pakhira,[d†] Raymond P. Welch,[a,†] Carlos Caicedo-Narvaez[b], Michael A. Luzuriaga[a], Bhargav S. Arimilli[a], Gregory T. McCandless[a], Babak Fahimi[b], Jose L. Mendoza-Cortes,[e,f,*] Jeremiah J. Gassensmith[a,c,*]

[a] Department of Chemistry and Biochemistry, [b] Renewable Energy and Vehicular Technology Laboratory, and [c] Department of Biomedical Engineering, The University of Texas at Dallas, 800 West Campbell Road, Richardson, Texas 75080, United States. [d] Discipline of Physics & Discipline of Metallurgy Engineering and Materials Science (MEMS), Indian Institute of Technology Indore (IIT Indore), Simrol, Khandwa Road, Indore-453552, Madhya Pradesh (M.P.), India. [e] Department of Chemical & Biomedical Engineering, FAMU-FSU joint College of Engineering, Tallahassee, Florida 32310, United States. [f]*Current address*: Department of Chemical Engineering & Materials Science, Michigan State University, East Lansing, Michigan 48824, United States.

[†] These authors contributed equally to this work.
* jmendoza@msu.edu
* Gassensmith@utdallas.edu

Summary

Solid state thermosalience—a sudden exertion of an expansive or contractive physical force following a temperature change in a solid state compound—is rare, few are reversible systems, and most of these are limited to a dozen or so cycles before the crystal degrades or they reverse slowly over the course of many minutes or even hours. In this work, we show a fully reversible actuator that is stable at room temperature for multiple years and is capable of actuation for more than two hundred cycles at near ambient temperature. Specifically, the crystals shrink to 90% of its original length instantaneously upon heating beyond 45 °C and expands back to its original length upon cooling below 35 °C. This temperature regime is important because it occurs around physiologically important temperatures. Furthermore, the phase transition occurs instantaneously, with little obvious hysteresis, allowing us to create real-time actuating thermal fuses that cycle between on and off rapidly.

Introduction

Materials that can transduce heat into well-defined and directed motion are rare but have a wide range of applications for a diverse array of technologies from microscopic pumps to energy harvesting. For instance, transducing well-defined thermally induced reciprocating actuation simply by taking advantage of the natural temperature fluctuation between day and night cycles is a possible way to harness ambient temperature changes into useful pollution-free electricity. In addition, the ever-increasing interest in the miniaturization of mechanical devices demands new actuating materials that can produce motion in the micron to millimeter regime. While actuators that operate from electrochemical *stimuli* are well-known,[1,2] the application of thermal expansion actuators has been limited by poor mechanical properties, material fatigue, or low coefficients of thermal expansion (CTEs). For instance, metallic aluminum and lead, which have the highest known CTEs in pure metals, are still in the regime of 20×10^{-6} K^{-1}. Thermo-responsive actuating

shape-memory polymers have been developed,[3-6] but they typically require a significant change in the global environmental temperature to actuate.[7]

Dynamic crystals are mechanically active single crystalline entities capable of amplifying small changes in molecular packing into large-scale anisotropic macroscopic motion. These materials—so-called thermosalient solids—have CTEs over an order of magnitude higher than the best pure-metals and undergo phase transitions at rates exceeding 10^5 times faster than non-thermosalient transitions.[8] This expansion is caused by a diffusionless "sergeants and soldiers" phase transition that is initiated at crystalline extremities and rapidly propagates throughout the crystal.[9,10] In some of these systems, expansion can cause a sudden single-crystal-to-single-crystal (SCSC) phase transition with substantial changes in unit cell size, thus providing even greater material expansion. Unfortunately, these SCSC events are typically irreversible and results in their destruction by splitting, jumping, or even dramatically exploding. These irreversible dynamic crystals have found applications as fuses[11], making use of their one-time ability to actuate to break a circuit; however, this irreversibility greatly limits their applications. In contrast to irreversible systems, there are very few reversible systems, and most of these are limited to a dozen or so cycles before the crystal degrades or they reverse slowly over the course of many minutes or even hours. Designing such systems is complicated by the fact that structure-function relationships in molecular crystals can be difficult to derive and thus *a priori* synthesis of actuating materials is challenging.

In this report, we show a thermosalient crystal, which is part of a family of thermosalient systems, that is a fully reversible actuator capable of more than two hundred cycles and room temperature stability for multiple years. The phase transition occurs instantaneously, with little obvious hysteresis, allowing us to create real-time actuating thermal fuses that cycle between on and off rapidly. Our family of actuating molecular crystals is based on a naphthalene diimide (NDI) core with alkoxyphenyl substituents (**Figure 1a**).[9] We have reported that the single-action thermosalient behavior is tunable across temperature ranges by altering the alkyl chain from four to nine carbons. [12] Here we report that, when the alkyl chain is 10 linear carbons, the thermosalient crystals show instantaneous reversible negative thermal expansion. Specifically, the crystals shrink to 90% of its original length instantaneously upon heating beyond 45 °C and, expand back to its original length upon cooling below 35 °C. This temperature regime is important because it occurs at a physiologically important temperature—at just the minimum temperature that can cause a burn in a finite amount of time—thus giving rise to use in thermal fuses to prevent skin burns from runaway thermal reactions in batteries or other portable electronics. It is also a convenient temperature range for extracting energy in the diurnal cycle of desert climates. Thus, we anticipate this family of materials may have a plethora of practical applications in addition to serving as a model for fundamental studies in structure-function behavior for heat conversion into mechanical energy.

Results and Discussion

After our discoveries that butoxyphenyl-NDI crystals[9] under temperature gradients exhibit irreversible thermosalience and reversible thermochromism, we expanded our search to other NDI derivatives based on alkyl chain length.[12] We hypothesize that longer chains and smaller ring overlaps might flatten the potential energy curve, thus facilitating the transition and improving the reversibility. Accordingly, we observe that this NDI family exhibits thermosalience and/or thermochromism across its many derivatives. Upon reaching 10 carbons (Decoxyphenyl-NDI; or DNDI for short), we find the crystal to be reversibly thermosalient, exhibiting negative thermal

expansion on heating past the phase transition point. What's more, the transition temperature is around 45 °C, a temperature range better-suited for physiologically and near normal temperature applications than other reversibly thermosalient crystals, which actuate at >80 °C[13,14] or lower than 0 °C.[15]

Table 1: Crystallographic parameters at 298K and 338K.

Parameter		298 K	338 K
Crystal System		Triclinic	
Space Group		$P\bar{1}$	
Formula		$C_{46}H_{54}N_2O_6$	
Unit cell	a (Å) =	5.232 (4)	8.775 (3)
	b (Å) =	7.643 (5)	9.070 (3)
	c (Å) =	25.120 (18)	29.218 (10)
	α (°) =	86.887 (19)	81.70 (2)
	β (°) =	87.346 (19)	83.383 (13)
	γ (°) =	80.28 (2)	63.15 (2)
Volume (Å^3)		987.8 (12)	2049.8 (12) Å^3
Crystal Color		Yellow	
Z		1	2
Reflections Collected		11522	33485
R_{int}		0.052	0.168
Density (g cm^{-3})[a]		1.229	1.184
w$R(F^2)$		0.177	0.280
Mo $K\alpha$ radiation, λ (Å)		0.71073	

[a]Although the unit cell volume nearly doubles, the number of units per cell (Z) also double, and the overall density decreases slightly, despite the fact that the bulk crystal decreases in volume significantly.

DNDI was synthesized based on literature protocols, substituting longer alkyl chains, and crystallized from the slow evaporation of chloroform. These crystals were examined with single crystal X-Ray diffraction at temperatures above and below the transition point, and the single crystal structure was solved across the operating temperature range. The crystallographic parameters are summarized in **Table 1**. Structural analysis indicates that the molecular arrangement within the lattice positions align the NDI cores parallel to each other with the alkyl chains fully extended away, forming layers of ribbon-like planes (**Figure 1b and c**). The centroid-to-centroid distances between the NDI cores shorten considerably with heating, and they pack together closer when the crystal's large axis of thermal contraction is arranged horizontally (**Figure 1c**). This is enabled by a change in the aromatic ring overlap, which causes a contraction of the linkers as temperature decreases. Upon heating past the transition point of 45 °C, the crystal shrinks to ~90% of its cold length in the long direction (**Figure 1e**). Put differently, the DNDI crystals were observed to have sudden negative thermal expansion at 45 °C. The width increases slightly and the there is no apparent change in thickness. The hot and cold lengths remain relatively stable (**Figure 1f**) following multiple cycles without loss in compressibility (**Movie S1**). Single crystal analysis shows that the cool and warm structures are two different crystal habits, both of which are triclinic, and differ only modestly in unit cell lengths and angles. This small change in packing may explain why the crystals are able to cycle without substantial degradation.

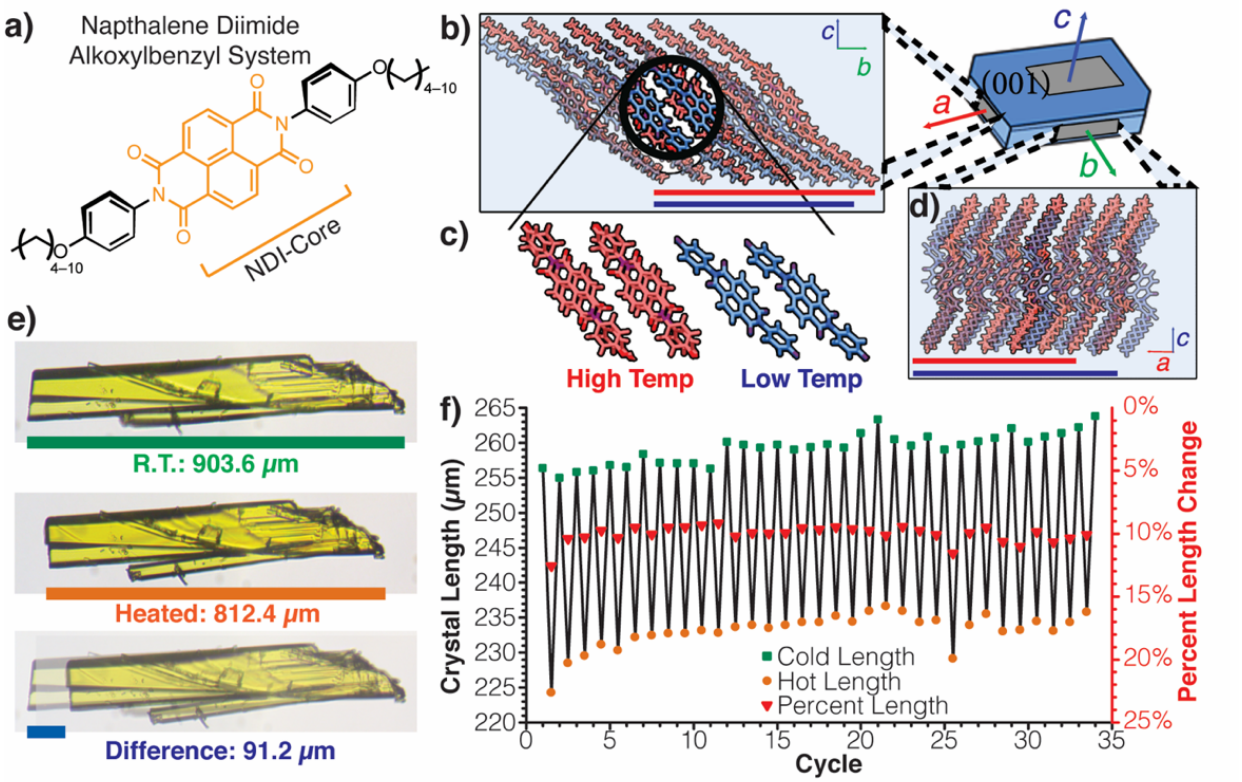

Figure 1. a) The structural formula of the Naphalene Diimide (NDI) systems, which all show thermosalient behavior. This work shows that when the alkyl chain is 10 carbons long (DNDI), the fluctuation becomes reversible. Overlap of both crystal phases at high (red) and low (blue) temperatures b) down the crystallographic *a*-axis, where the expansion along the *b*-axis and *c*-axis from packing is illustrated. c) A Zoom-in into the ring overlaps down the *a*-axis shows the NDI core and phenoxyl ring overlap becomes slip stacked at high temp and d) down the crystallographic *b*-axis, where the expansion at low temperature is obviated. e) Optical micrographs of a DNDI crystal at room temperature (top), heated (middle) and an overlay illustrating the length difference (bottom). f) Graph showing crystal length changes of a single crystal over 34 thermal cycles from cold (green squares) to hot (orange circles) and back with percent length change (red triangles).

We conducted differential scanning calorimetry on bulk DNDI crystals cycling the temperature from 20 °C to 60 °C and back for 200 cycles (**Figure 2a**). The exothermic and endothermic peaks show no shift in temperature, width, or height over the cycles, indicating that the bulk molecular rearrangement is not attenuated. The recovered crystals were apparently thinner, having slightly delaminated in the DSC though the recovered crystals continued to actuate at the same temperatures with the same 10% decrease in length. One such recovered crystal is shown in the insert of **Figure 2a**.

DSC analysis coupled with computational efforts give some insight into the crystal transformation. The endothermic contraction process, which is at its most endothermic at 46.3 °C, occurs with a ΔG of -6.2×10^3 J/mol, a ΔH -7.7×10^3 J, and an entropic penalty of $\Delta S = -35$ J/mol•C. Conversely, the "expansion" process is ΔG of $+6.0\times10^3$ J/mol at 33.3 °C—the exothermic peak maximum. The reverse process appears largely entropy driven, with a $\Delta S = 59$ J/mol•C and a ΔH 8.0×10^3 J/mol. The slight discrepancy in free energy between these transitions may arise from the thermal delamination of the crystals.

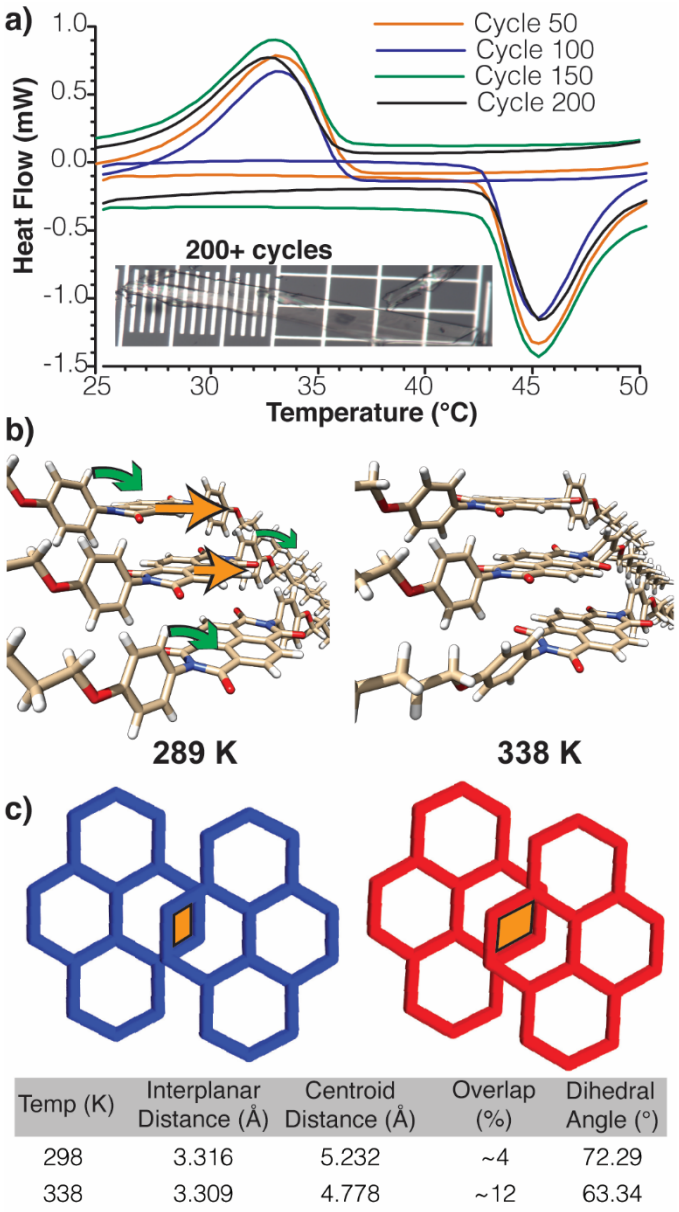

Temp (K)	Interplanar Distance (Å)	Centroid Distance (Å)	Overlap (%)	Dihedral Angle (°)
298	3.316	5.232	~4	72.29
338	3.309	4.778	~12	63.34

Figure 2. a) DSC traces of DNDI are shown for 50, 100, 150, and 200 cycles. The inset shows a single DNDI crystal from the DSC experiment, which remains ~800 μm long, after 207 cycles. Major divisions of the scale are 100 μm. b) The dynamic motions that DNDIs undergo from the low temperature phase to the high temperature phase involve a rotation of one of the two aromatic rings on each NDI (green arrow) to allow the NDI cores to move over each other (orange arrow). c) While the rotation of the aromatic ring is energetically uphill, the greater pi-overlap in the high temp structure is a lower energy structure at these temperatures with the distances and angles tabulated.

To support and explain our experimental observations, we conducted *DFT* calculations[16,17] considering the periodic crystal structure and molecular model systems (Figure S1, S2). The crystal structure of the DNDI crystal (Figure S1a, S2a), and the molecular clusters models have been used to estimate the different local and non-local effects. More specifically, we studied different molecular models surrounded by 1-3 layers to study the neighboring effect (Figure S1b-e, S2b-e). Thermochemistry calculations were performed at 298K and 333K in all these crystal structures

and molecular clusters. Our calculations reveal that ΔH^{theory} = 7.2–8.7 x 10^3 J/mol for DNDI surrounded by mono-, bi- and tri-layer molecules. This is excellent in agreement with the experimental value (ΔH^{exp} = 7.7–8.0 x 10^3 J/mol). The entropy changes from our theoretical calculations, ΔS^{theory} = 53.0–54.3 J/mol•C for the same molecular models is likewise in agreement with the experimental values (ΔS^{exp} = 35–59 J/mol•C). In order to understand the barriers to switch from one form to the other, we hypothesize that the driving force for the phase transition is a lower energy co-facial π-π overlap of the NDI cores. This better overlap is inhibited at low temperature by the steric the bulky aromatic rings. Only when there is enough thermal energy for these rings to rotate out of the way, can the NDI cores move closer to each other. To test this hypothesis, a scan was performed on the rotation of the linker (Figure S3). The estimated electronic rotational barrier, $\Delta E^{\dagger}$ = 13.6 – 14.4 kJ.mol^{-1}, which is not much higher than the available thermal energy at the phases transition. Thus, we postulate that a possible mechanism driving the phase transition is the greater thermal energy to permit movement of the rings; analogous to two butterflies flying next to each other. In other words, a full rotation of the rings is not necessary, but the available thermal energy allows for the rings to be perturbed enough to affect the π-π interaction. In summary, the overall global motion and experimental thermodynamic data support that an energetically penalizing rotation of the aromatic ring must occur to allow the NDI cores to slide over each other (Figure 2b), which offers greater stabilization from improved overlap of the NDI π-systems (Figure 2c). These results are consistent with the fact that our *n*-phenoxyl substituted NDI systems containing four, seven, eight, and nine carbons likewise undergo thermosalience. Indeed, more than 820 solid state structures of functionalized NDI cores have been uploaded to the Cambridge Structural Databased and many experimentally tested as organic semiconductor systems, yet only the derivatives featuring an *n*-phenoxyl substituent have demonstrated thermosalient behavior. Therefore, the importance of the aromatic ring cannot be understated.

The single-crystal-to-single-crystal transition occurs with a slight change in unit cell parameters, which contributes to a difference in cellular birefringence. We were able to use this change in birefringence to better understand the mechanism of actuation. During a gradual thermal gradient, the transition occurs slowly, nucleating at a certain point along the crystal long axis while all of the molecules in a line rearrange. The "wavefront" (**Figure 3, red diagonal lines**) then propagates lengthwise as a solid line in either direction down the crystal (**Figure 3, yellow arrows**). At crystal imperfections, cracks, or dislocations, the wave front can stall, and the stress lines become apparent. The thermal gradient takes a bit longer to affect the other side of the obstacle, during which the wavefront above or below the disturbance may continue propagating past, causing the crystal to split disjointly until the wave fronts catch up and the sections merge again (**Movie S2**). The most common method of crystal splitting in this manner is along the plane parallel to the large [001] face, causing delamination of the parallel sheets. Repeated thermal cycles tend to cleave or shear the crystal into thinner crystals that continue to actuate. Intriguingly, the phase transition can occur at any point in the crystal and occasionally at multiple locations. These phase transitions presumably follow a "sergeants and soldiers" propagation wherein the phase transition induces the transition nearby.

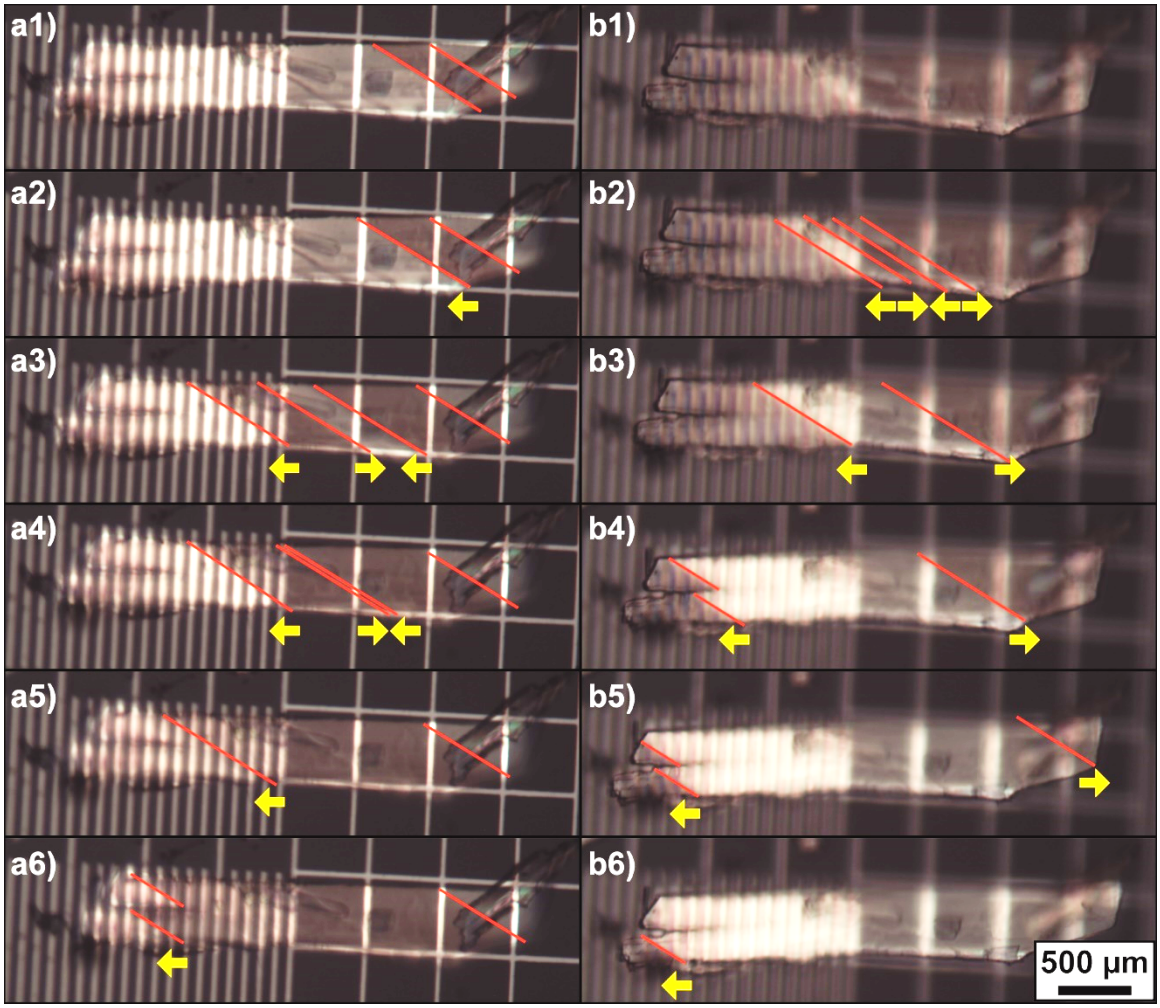

Figure 3. Still frames of DNDI crystal under polarized light after 200 thermal cycles subjected to a slow thermal gradient. Propagation (yellow arrows) of the molecular rearrangement wavefronts (red lines) through the long axis of the crystal upon a1-6) heating and b1-6) cooling past the respective thermal transition points.

To take advantage of this thermosalience, inspiration was drawn from Khalil et al.[11] to coat the crystal in a conductive silver layer for use in an electronic circuit. DNDI exhibits no conductivity in its natural state, so a conductive coating is required to allow current to pass through. Selected large DNDI crystals were metallized via the Tollens Silver Mirror reaction and examined by scanning electron microscopy (SEM) (**Figure 4a**). A thin uniform coating of silver nanoparticles was found on the crystal surface and the crystals were visually grey and shiny instead of their usual yellow. Attempts to close a circuit with these crystals failed because the silver coating was not thick enough, and the silver mirror reaction was redone on the same crystals. As the silver coating grew thicker, the silver particles merged into a solid sheet. The coating appeared to have a higher affinity for itself than to the crystal surface, and upon thermal transition of the crystal, the silver coating delaminated from the crystal but remained intact (**Movie S3**). However, these crystals successfully closed a circuit and were deemed conductive enough to proceed.

The conductive crystals were connected in an electronic circuit (**Figure 4b**) to bridge a gap of a width such that it is smaller than a cold crystal but larger than a hot one. Initial attempts using copper electrodes resulted in intermittent conduction at best, as there was not very good contact

between the crystal and the copper electrodes. Filter paper soaked in saturated sodium chloride as a liquid electrolyte solution was found to work well. Before coating with silver the DNDI crystals show no electrical conductivity whatsoever, so any electrical measurements are entirely based on the nature of the coating. Upon passing a current through the coated crystal, the silver coating visibly turned black moving from the negative to the positive end of the crystal (**Movie S4**). Once the current provided enough heat to the circuit path—either the silver coating or the liquid electrolytes—the crystal contracted.

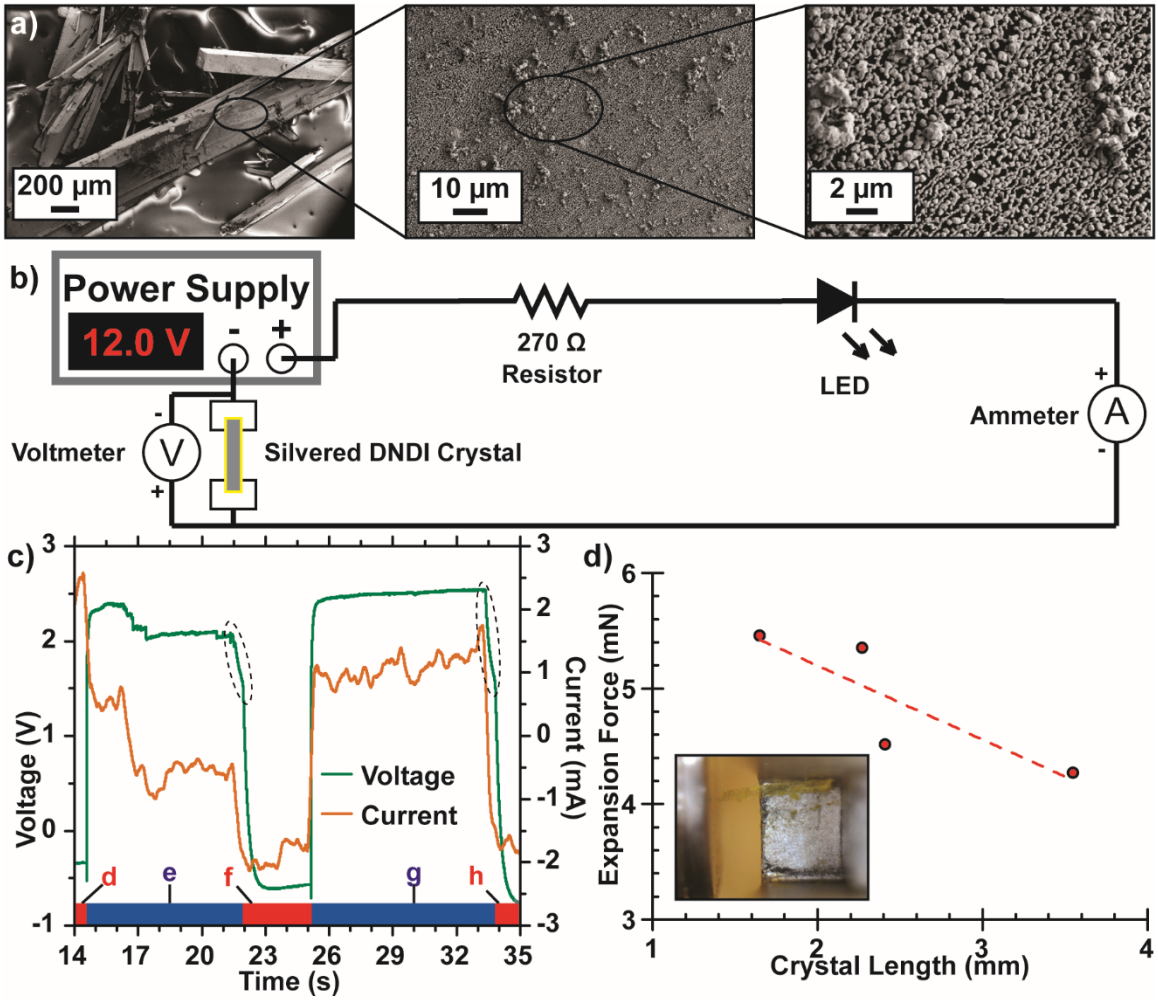

Figure 4. a) Scanning Electron Micrographs of silvered DNDI crystals at progressively higher magnifications. At higher magnification, left-to-right, individual silver nanoparticles are visible. b) Circuit schematic for electrical actuation. c) Oscilloscope traces of the measured voltage and current through the circuit over time. At the bottom, the red sections represent the time the crystal was expanded, and the blue sections represent the time the crystal was contracted. The dotted black ellipses on the voltage trace indicate the capacitor discharge in the power supply upon turning off the voltage. d) Force-length comparison of 4 DNDI crystals. The inset shows a crystal (yellow) resting on the aluminum heatsink with the backstop on the right and the sensor on the left.

On applying or removing the voltage, the crystal rapidly responded by contracting or expanding, respectively (**Supplemental Movies**). If the crystal is placed properly, the heating and cooling

induces a pulsive effect as the crystal heats, shrinks, and shorts the circuit. The crystal then cools, expands, and closes the circuit. Analysis of the motion shows that we were able to obtain expansion-re-expansion rates between 1–2 Hz, which is exceptionally rapid for organic crystals. On turning off the power supply, the voltage drops slowly at first, then rapidly to the baseline, indicated by the dotted ellipses in **Figure 4c**. This is because the capacitors in the power supply are discharging briefly after turning the voltage off.

Re-expansion force measurements were obtained using a piezoelectric sensor placed against a heated crystal and measuring the voltage produced by the piezoelectric material in response to the crystal pushing into it (**Figure 4d**). This voltage can be converted to force once the physical parameters of the sensor are determined. The crystals selected were difficult to align and register any force, but the force output was plotted against the crystal length for four crystals in a range of ~1.5 to ~3.5 mm. The forces registered in a range of ~4 to ~5.5 mN show a loose inverse proportion with length. However, the crystals tend to break apart under resistance to expansion. This suggests that the internal forces holding the [001] planes together are weaker than the outward expansion force, as the energy required to push outwards instead shears the crystal along its plane.

In summary, we have shown that DNDI can be used as a thermally activated actuator for use as an electrical switch or indicator, reusable over many cycles in ambient and near physiologically important temperatures. These crystals retain their actuation capability even after breaking into smaller parts and show promising potential for use embedded in an elastic matrix that can align and magnify the expansive capabilities of DNDI for use as a thermal-actuated sensor, muscle, extracting energy in the diurnal cycle of desert climates, or in thermomechanical automatic devices. These crystals have potential to impact the fields of electronics and micromechanics in different directions.

Methods

Synthesis of DNDI

DNDI was synthesized based on literature protocols,[12,18] purified by silica column chromatography in isocratic chloroform, and crystallized by evaporation from the fraction tubes.

Metallization of DNDI

Sufficiently large DNDI crystal candidates were selected and added to a scintillation vial with 5 mL silver nitrate, 200 mg glucose, and 5 drops ammonium hydroxide, and gently heated while swirling to around 50 °C until the silver mirror began to form. The vial was then left on a rotisserie at room temperature for 2 days and then vacuum filtered while rinsing with ultrapure water and drying.

Circuit Design

A circuit was set up and soldered to a breadboard consisting of a terminal for power supply, a 270 Ω resistor, a red LED, terminals for current measurement, electrodes for the crystal switch contacts, and a terminal for return power supply. The crystal switch contacts consisted of filter paper strips moistened by saturated sodium chloride solution and mounted above acrylic blocks with an air gap for the crystal to bridge without electrolytes causing a short circuit. The LED indicated a closed circuit, the resistor protected the LED from overcurrent, and the current was monitored as the power supply voltage was increased until the crystal actuated. The metallized crystal actuation was monitored with a USB microscope.

Force Measurements

Prior to coating with silver, crystals were placed between the fins of an aluminum heatsink with a machined steel rod as an adjustable backstop on one end and a Honeywell FSG005WNPB force sensor on the other, and a thermocouple glued to the outside of the fins. The system was heated by direct contact with a soldering iron tip at 800 °C until the crystal contracted. The force sensor and backstop were adjusted such that the crystal was butted up against both and would press against the sensor upon re-expansion. The system was then cooled by direct contact with an ice cube on the underside of the heatsink until the crystal expanded into the force sensor. The voltage change was recorded and converted to force according to the sensor properties listed in the manufacturer's datasheet.

Computational Details:

Due to the extended nature of the bulk DNDI crystal structure, the periodic crystal structures (Figure S1a, S2b) and four cluster modeling systems with 1-4 layers were used (Figure S1b-d, S2b-d). The equilibrium structures, geometries, calculations of energetics and rotational barrier of the model systems of the DNDI crystal were obtained with the hybrid unrestricted density functional theory (DFT) with the UB3LYP-D3 level of theory using correlation-consistent polarization double ζ-quality basis sets for all atoms.[16,17] The vibrational frequencies at the optimized geometries were analyzed to confirm ground states. The thermochemical calculations were performed at 298K and 333K corresponding to each crystal structure configuration. The rigid scan was performed by considering the same models (Figure S3). The threshold used for evaluating the convergence of the energy, forces, and electron density was 10^{-7} a.u. for each parameter. All calculations were performed with the Gaussian09 quantum chemistry code. The details of the computations can be found in the Supporting Information.

Data Availability

Crystal structure data that support the findings of this study have been deposited in the CCDC with the accession codes CCDC 1992519-1992523. These data can be obtained free of charge via www.ccdc.cam.ac.uk/data_request/cif, or by emailing data_request@ccdc.cam.ac.uk, or by contacting The Cambridge Crystallographic Data Centre, 12 Union Road, Cambridge CB2 1EZ, UK; fax: +44 1223 336033.

References

1 Otero, T. F. & Sansieña, J. M. Soft and Wet Conducting Polymers for Artificial Muscles. *Advanced Materials* **10**, 491-494, doi:10.1002/(sici)1521-4095(199804)10:6<491::aid-adma491>3.0.co;2-q (1998).

2 Okuzaki, H. & Osada, Y. Electro-driven chemomechanical polymer gel as an intelligent soft material. *Journal of Biomaterials Science, Polymer Edition* **5**, 485-496, doi:10.1163/156856294X00167 (1994).

3 Peterson, G. I., Dobrynin, A. V. & Becker, M. L. Biodegradable Shape Memory Polymers in Medicine. *Advanced Healthcare Materials* **6**, 1700694, doi:10.1002/adhm.201700694 (2017).

4 Ge, F. & Zhao, Y. A new function for thermal phase transition-based polymer actuators: autonomous motion on a surface of constant temperature. *Chemical Science* **8**, 6307-6312, doi:10.1039/C7SC01792H (2017).
5 Zhao, Q., Zou, W., Luo, Y. & Xie, T. Shape memory polymer network with thermally distinct elasticity and plasticity. *Science Advances* **2**, e1501297, doi:10.1126/sciadv.1501297 (2016).
6 Wang, J. *et al.* Tunable shape memory polymer mold for multiple microarray replications. *Journal of Materials Chemistry A* **6**, 24748-24755, doi:10.1039/C8TA04763D (2018).
7 Zhao, Q., Wang, Y., Cui, H. & Du, X. Bio-inspired sensing and actuating materials. *Journal of Materials Chemistry C*, doi:10.1039/C9TC01483G (2019).
8 Panda, M. K. *et al.* Colossal positive and negative thermal expansion and thermosalient effect in a pentamorphic organometallic martensite. *Nature Communications* **5**, 4811, (2014).
9 Dharmarwardana, M. *et al.* Thermo-mechanically responsive crystalline organic cantilever. *Chem. Commun. (Cambridge, U. K.)* **53**, 9890-9893, doi:10.1039/C7CC04346E (2017).
10 Panda, M. K. *et al.* Strong and Anomalous Thermal Expansion Precedes the Thermosalient Effect in Dynamic Molecular Crystals. *Scientific Reports* **6**, 29610, (2016).
11 Khalil, A., Ahmed, E. & Naumov, P. Metal-coated thermosalient crystals as electrical fuses. *Chem. Commun. (Cambridge, U. K.)* **53**, 8470-8473, doi:10.1039/C7CC04251E (2017).
12 Dharmarwardana, M. *et al.* The thermo-responsive behavior in molecular crystals of naphthalene diimides and their 3D printed thermochromic composites. *CrystEngComm* **20**, 6054-6060, doi:10.1039/C8CE00798E (2018).
13 Alimi, L. O., van Heerden, D. P., Lama, P., Smith, V. J. & Barbour, L. J. Reversible thermosalience of 4-aminobenzonitrile. *Chemical Communications* **54**, 6208-6211, doi:10.1039/C8CC03636E (2018).
14 Lončarić, I. *et al.* Reversible Thermosalient Effect of N′-2-Propylidene-4-hydroxybenzohydrazide Accompanied by an Immense Negative Compressibility: Structural and Theoretical Arguments Aiming toward the Elucidation of Jumping Phenomenon. *Crystal Growth & Design* **17**, 4445-4453, doi:10.1021/acs.cgd.7b00785 (2017).
15 Karothu, D. P., Weston, J., Desta, I. T. & Naumov, P. Shape-Memory and Self-Healing Effects in Mechanosalient Molecular Crystals. *Journal of the American Chemical Society* **138**, 13298-13306, doi:10.1021/jacs.6b07406 (2016).
16 Grimme, S., Antony, J., Ehrlich, S. & Krieg, H. A consistent and accurate ab initio parametrization of density functional dispersion correction (DFT-D) for the 94 elements H-Pu. *The Journal of Chemical Physics* **132**, 154104, doi:10.1063/1.3382344 (2010).
17 Becke, A. D. Density-functional thermochemistry. III. The role of exact exchange. *The Journal of Chemical Physics* **98**, 5648-5652, doi:10.1063/1.464913 (1993).
18 Fomine, S., Fomina, L., Arreola, R. & Alonso, J. Bisimide-lactamimide ring contraction in six-membered polyimides. *Polymer* **40**, 2051-2058,

Supplementary Information

Supplementary Information is linked to the online version of the paper at [future link]

Acknowledgements

J.J.G. would like to acknowledge National Science Foundation [CAREER DMR-1654405], the Welch Foundation [AT-1989-20190330], and the ACS Petroleum Research Fund [57627-DNI10] S. P. acknowledges the support from the SERB-DST, Government of India for providing the Ramanujan Faculty Fellowship under the Grant No. SB/S2/RJN-067/2017 and Early Career Research Award (ECRA) under the Grant No. ECR/2018/000255.

Author Contributions

DNDI was synthesized by M.D. and B.S.A. Single Crystal X-Ray Diffraction was performed by G.T.M. Hot-stage and polarized optical microscopy, silver metallization, SEM, circuit design and construction, and primary manuscript draft writing were performed by R.P.W. DSC was performed by M.A.L. Heatsink machining and construction were performed by C.C. Electrical and force measurements were performed by R.P.W. and C.C. Quantum calculations and theoretical models were performed by S.P. and designed by J.L.M-C. Electrical measurement space and equipment were provided by B.F. Funding was provided by J.J.G. Manuscript editing was performed by R.P.W., J.L.M-C., and J.J.G.

Author Information

The authors declare no competing interests.
Correspondence and requests for materials should be addressed to gassensmith@utdallas.edu or jmendoza@msu.edu